Journal of Non-Crystalline Solids 639 (2024) 123090

Contents lists available at ScienceDirect

Journal of Non-Crystalline Solids

journal homepage: www.elsevier.com/locate/jnoncrysol

Amorphous boron carbonitride (BC_4N) from ab initio simulations

Murat Durandurdu

Department of Nanotechnology Engineering, Abdullah Gül University, Kayseri, Türkiye

ARTICLE INFO

Keywords:
Amorphous
Boron carbonitride
Graphite-like
ab initio

ABSTRACT

This study utilizes ab initio molecular dynamics simulations to explore the structure and properties of amorphous boron carbonitride (a-BC_4N). A 432-atom model, generated via a conventional melt-and-quench technique, exhibits a graphite-like structure with all elements possessing an average coordination number of about 3.0. C atoms dominate within individual layers, interspersed with distinct BN domains. This atomic arrangement deviates considerably from that proposed for crystalline BC_4N structures. Despite this structural variation, the a-BC_4N model is likely a narrow band gap semiconductor (0.15 eV), similar to its crystalline counterparts. In terms of mechanical properties, a-BC_4N demonstrates similarities with various layered materials while exhibiting a notably larger bulk modulus.

1. Introduction

Significant efforts have been devoted to investigating ternary boron carbonitride (BCN) materials due to their diverse structures and promising applications [1-3]. The structural topology and composition of these materials play a crucial role in defining their properties [1-3]. The hybrid BCN system, which combines graphite (a semimetal) and hexagonal BN (a semiconductor), exhibits excellent semiconducting properties [4,5]. In terms of bonding, BCN materials can be categorized into two main types based on their structure: sp^2 bonded BCN materials possess graphite-like structures, characterized by trigonal coordination of atoms while sp^3 bonded BCN materials have diamond-like structures, featuring tetrahedral coordination of atoms.

Graphite-like BC_4N crystal (g-BC_4N) has acquired less research attention compared to other materials in the BCN family. The initial exploration into BC_4N involved its synthesis through a chemical process, and analysis of the infrared spectrum led to the proposition of a "sandwich" structure [6]. This hypothetical structure resembled a layered material with a central BN layer sandwiched between two flanking graphite layers. Later studies successfully produced BC_4N with a graphitic structure, but this time through a different reaction process involving low surface area carbon and a mixture of urea and boric acid at high temperatures (930 °C) [7]. The resulting material possessed a composition close to the ideal BC_4N formula. However, unlike the earlier proposition of a distinct BN core, this BC_4N exhibited a layered structure with a key difference: a random distribution of B, C, and N atoms within these layers. The same study employed first-principles calculations to predict the electronic properties of g-BC_4N and revealed that g-BC_4N, regardless of the specific arrangement of B and N atoms, exhibits semiconducting behavior. The predicted band gap was found to range from 0.17 to 1.1 eV depending on the specific atomic ordering. This finding highlights the potential of g-BC_4N for various electronic applications.

Building upon the experimental procedure outlined in Ref. 6, Solozhenko et al. investigated the thermal stability of g-BC_4N under high pressure and temperature environments [8]. The study revealed that g-BC_4N underwent decomposition into different phases depending on the applied pressure and temperature conditions. At specific conditions, g-BC_4N decomposed into a mixture of BN and amorphous graphite (a-graphite) phases. Under different pressure and temperature settings, the decomposition yielded cubic BN and a-graphite structures.

In a different study, first-principles calculations were conducted to predict the most stable structure and electronic properties of g-BC_4N [9]. These calculations proposed that a specific BC_4N structure, with one layer of B-N atoms stacked between two layers of C—C atoms, exhibited the lowest overall energy among various modeled configurations. The calculations also predicted semiconducting behavior for g-BC_4N with a narrow band gap of approximately 0.05 eV.

On the contrary, there has been a growing interest in sp^3-bonded diamond-like BC_4N (d-BC_4N) structures owing to their potential as hard materials with exceptional mechanical properties. Experimental synthesis of d-BC_4N has demonstrated a high Vickers hardness ranging from 68 to 85 GPa [10,11]. Moreover, theoretical investigations utilizing diverse algorithms have put forth several d-BC_4N structures, some of which display remarkable mechanical characteristics [12-15]. Additionally, these d-BC_4N structures have been recognized as semiconductors, broadening their potential applications beyond hardness

E-mail address: murat.durandurdu@agu.edu.tr.

https://doi.org/10.1016/j.jnoncrysol.2024.123090
Received 11 April 2024; Received in revised form 11 June 2024; Accepted 13 June 2024
Available online 25 June 2024

considerations.

Amorphous BC_4N (a-BC_4N) has been successfully synthesized through various methods. One approach involved the thermal conversion of pyridine-borane [16]. a-BC_4N ceramics underwent decomposition into graphite and BN phases when subjected to temperatures of 500 °C and pressures ranging from 5 to 12 GPa [17]. The ball milling of BN and graphite has also been demonstrated to yield a-BC_4N [10]. Indeed, experimental synthesis of d-BC_4N was achieved through high-pressure and high-temperature treatment of the a-BC_4N structure at 20 GPa and 2200 K [10].

To the best of our knowledge, the atomic structure, as well as the mechanical and electrical properties, of a-BC_4N have not been investigated in existing literature. Therefore, the primary objective of this computational study is to provide insights into a-BC_4N in order to address this gap in the current literature. By conducting comprehensive computational analyses, we aim to contribute valuable information regarding the atomic arrangement and properties of a-BC_4N, thereby advancing the understanding of this

2. Method

Our investigation utilized an ab initio approach based on density functional theory (DFT) to explore the properties of a-BC_4N [18]. The well-established Troullier-Martins scheme was employed [19] to contract pseudopotentials. We adopted double zeta (DZ) basis sets and performed calculations using the Γ-point. The widely used Perdew-Burke-Ernzerhof (PBE) generalized gradient approximation (GGA) functional [20] was employed in conjunction with Grimme's dispersion correction [21] to account for weak interactions between atoms. A mesh cutoff energy of 150 Ry was chosen to determine the Hartree and exchange-correlation contributions to the total energy. Molecular dynamics (MD) simulations were conducted using a time step of 1.0 fs within the isothermal–isobaric ensemble (NPT). For temperature control, velocity scaling was employed, while the Parrinello-Rahman technique [22] was utilized to maintain zero-pressure during the simulations. We used sp^3 bonded orthorhombic (Imm2) crystal [14] as the initial structure and created a configuration with 432 atoms. This initial model was subjected to a high temperature of 7000 K for 5.0 ps to simulate a melting process, followed by cooling to 4500 K, where the system was equilibrated for 50 ps. To verify that the structure exhibits characteristics of a melt at 4500 K, we performed an additional 1000 molecular dynamics (MD) steps and calculated the mean-square displacement (MSD) of the atoms. The calculated MSD is presented in Fig. 1. Beyond 200 femtoseconds (fs), the MSD exhibits a linear behavior, which is indicative of a diffusive state in the BC_4N melt. To quantify the diffusion coefficient (D), we performed a linear fit on the MSD data between 200 fs and 600 fs. Using Einstein's relation, $\langle (r(t) - r(0))^2 \rangle = 6tD$ the diffusion coefficient D was estimated to be approximately 7.8×10^{-8} m^2/s. This value suggests that the structure indeed exhibits the characteristics of a melt at this temperature. Subsequently, the system was gradually cooled using a quenching rate of 1×10^{13} K/s. At 4000 K, the system underwent another equilibration step for 50 ps before being quenched to 300 K using the same quenching rate. During the MD simulation, no shear deformation was allowed and the simulation box was kept orthogonal. Finally, the system was relaxed using the variable cell conjugate gradient method until the forces acting on the atoms became negligible (less than 0.01 eV/Å). During this process, both the atomic positions and the volume, including the shape of the simulation box, were allowed to relax. The resulting volume of the structure is 3686.355 $Å^3$, with supercell parameters $a = 20.385$ Å, $b = 12.503$ Å, and $c = 14.465$ Å. The cell angles are $\alpha = 91.06°$, $\beta = 89.708°$, and $\gamma = 90.504°$ To achieve a more accurate estimation of the band gap energy, we employed GGA+U calculations. Using recent HSE06 hybrid functional calculations on d-BC_4N with the Cmc21 crystal structure [15] as a reference, we determined a Hubbard potential (U) value of 3.75 eV for C-p, yielding a band gap energy of 5.68 eV for the Cmc21 crystal. This value closely aligns with the finding of 5.62 eV [15]. We applied this parameter across the amorphous configuration to predict its electronic structure. It should be noted here that the GGA+U calculation was used solely to estimate the electronic structure of the amorphous configuration. Partial analysis of the structures was conducted using the ISAACS program [23]. The atomic-level visualization of the amorphous structure was conducted using VESTA software [24].

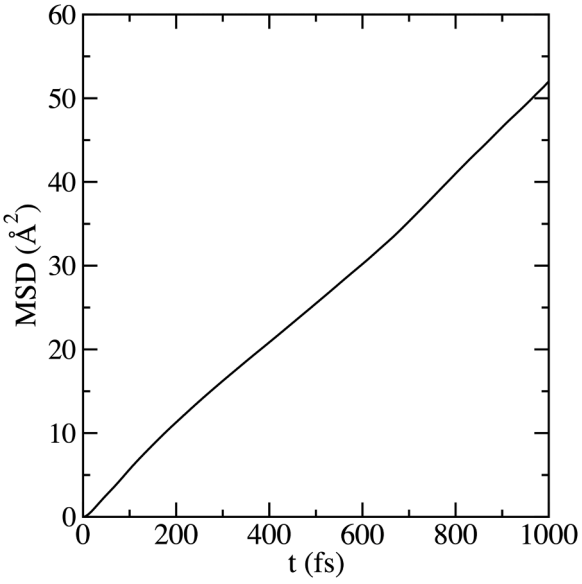

Fig. 1. Mean-square displacement at 4500 K.

3. Results

Fig. 2 illustrates a ball-and-stick model of the simulated BC_4N material. This model reveals a layered structure, where a few atoms directly connect to these layers. The a-BC_4N material appears to differ from the proposed sandwich-like arrangement or random distribution of B, C, and N atoms in crystal structures [6,7]. In amorphous network, C atoms dominate each layer, but there are also regions with BN domains. It seems that CN and BC domains are less prevalent in this structure. The average distance between adjacent layers is approximately 3.2 Å and the calculated density of the simulated amorphous structure is 2.3459 g/cm^3, which is in the range of 2.31–2.78 g/cm^3 reported for g-BC_4N [9]

To gain further insights into the local structure of the amorphous configuration, partial pair distribution analysis is conducted, with the results depicted in Fig. 3. This analysis exposes bonding interactions among all species, excluding N—N bonds. Given the prevalence of C

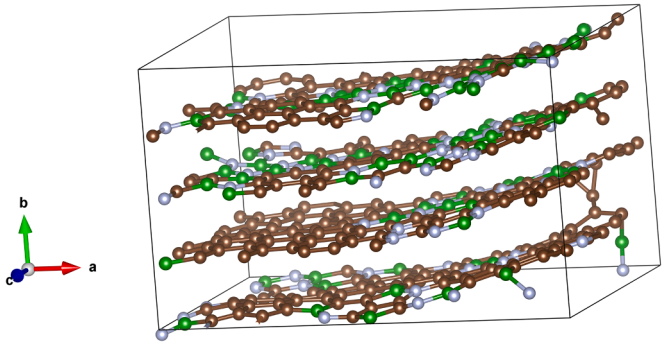

Fig. 2. Ball-stick representation of the a-BC_4N model. Brown, green, and gray colors represent C, B, and N atoms, respectively. The supercell parameters *a, b*, and *c* correspond to the *x, y*, and *z* directions, correspondingly.

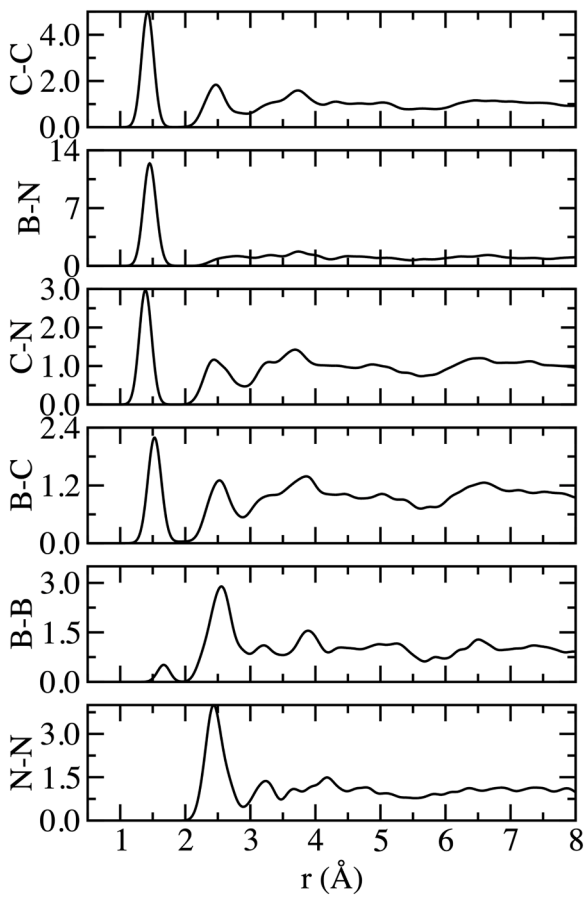

Fig. 3. Partial pair distribution functions (PPDFs) of the amorphous configuration.

atoms in the structure, the initial focus is on C—C bonding, occurring at a distance of 1.42 Å. This measurement closely mirrors the 1.42 Å reported for a-graphite [25,26]. Regarding B-N bonds, the bond length is approximately 1.45 Å, aligning well with the 1.44 Å observed in BN structures [27]. The separation distance between C and N atoms is determined to be 1.39 Å, falling within the typical range of 1.30 Å to 1.463 Å observed in crystalline and amorphous CN structures [28,29]. A B-C separation distance of 1.53 Å is observed, comparable to values in the BC_5 (1.51 Å) [30] and BC_3 (1.55) [31] crystals in theoretical studies. The B-B bond length is measured at 1.66 Å, notably shorter than the 1.76 Å reported for a-BC_5 [32].

A detailed analysis of the atomic bonding within the simulated a-BC_4N model is conducted to understand the local atomic environment. Cutoff method is employed to determine the coordination numbers of each atom type. This method defines specific bond length thresholds for each atomic pair (B-*B* = 1.95 Å, B-C = 1.91 Å, C—C = 1.83 Å, B-*N* = 2.01 Å and C—*N* = 1.81 Å) to identify bonding interactions. The analysis reveals interesting trends in the coordination preferences of each element. The majority C atoms (around 98.6 %) exhibit threefold coordination and the remaining small fraction (1.39 %) forms four bonds. On average, a C atom participates in 3.013 bonds, with a strong preference for bonding with other C atoms (C—C: 2.347). However, some C atoms also bond with B (C-B: 0.329) and N (C—N: 0.336). Similar to C, most B atoms (around 97.2 %) exhibit threefold coordination, with a minor fraction (2.78 %) having four bonds. The average coordination number for B is 3.013. B atoms favor bonding with N (B-N: 1.611) and C (B-C: 1.319). Interestingly, there is very little B-B bonding observed (B-B: 0.083). N atoms follow a similar trend, with approximately 96 % exhibiting threefold coordination and the remaining 4.17 % having two bonds. The average coordination number for N is also 2.958. Like B, N atoms primarily bond with B (N-B: 1.611) and C (N—C: 1.347).

While the coordination analysis provides a general picture of bonding preferences, a more detailed analysis of the local atomic arrangements is available from the chemical environment investigation presented in Table I. This investigation identifies the most prevalent bonding configurations surrounding each element type. For C atoms, the analysis reveals that C—C_3 is the most common configuration (51 %), followed by C-BC_2 at 17 % and C—NC_2 at 14 %. This suggests that nearly half (49 %) of C atoms form bonds with either B or N atoms. The analysis of B environments provides a more nuanced picture: B-N_2C is the most prevalent configuration at 33 %, followed by B-NC_2 at 17 %. It is crucial to note the presence of B-N_3 at around 15.28 %, emphasizing the preference of B for N neighbors. Similarly, the analysis of N environments reveals N-B_2C at 45 % and N-BC_2 at 32 % as the prevalent configurations. Like B, the analysis highlights the dominance of N-B_3 at around 12.50 %. The chemical environment analysis and visualization of the model offers valuable insights into the local atomic arrangements within a-BC_4N. It exposes distinct regions rich in C and BN domains, based on the prevalence of bonding motifs like C—C_3, B-N_3, and N-B_3. However, the analysis does not show significant BC or CN domains within the structure, suggesting these specific arrangements are less favorable.

The analysis of the atomic structure extends to the examination of bond angle distribution functions. Several distributions are depicted in Fig. 4, each displaying a principal peak near 120°, indicating prevalent trigonal symmetry. Additionally, the presence of five-, seven-, and eight-membered rings, akin to those found in a-graphite, results in angles near the hexagonal angle. This observation is further supported by the ring statistical analysis presented in Fig. 5, which highlights the abundance of six-membered (hexagonal) rings, followed by five and seven-membered rings.

The electron density of states (EDOS), a crucial indicator of electronic properties, is calculated using the GGA+*U* method. Fig. 6 depicts the resulting EDOS for the simulated a-BC_4N model. In the figure, the Fermi level is shifted to zero-eV and a Gaussian broadening of 0.085 eV is used to plot the EDOS. The EDOS for the amorphous structure lacks a clear forbidden gap, indicating a semimetallic nature of the EDOS. However first-principles calculations suggest that g-BC_4N can be a narrow band gap semiconductor and exhibit band gap values ranging from 0.05 to 1.1 eV, depending on the arrangement of C, B, and N atoms [7,9]. Therefore, the band gap energy of a-BC_4N can be as small as in the crystals, making it challenging to clearly represent in the EDOS due to Gaussian broadening. Therefore, attention shifts to the energy difference between the highest occupied molecular orbital (HOMO) and the lowest unoccupied molecular orbital (LUMO) states, revealing a difference of 0.15 eV. This value closely aligns with the range observed in the BC_4N crystals, suggesting that despite structural disorder and the formation of various bond types in the amorphous network, the electronic properties remain relatively consistent. For comparison, the electronic structure of a-BC_5, another material with a similar EDOS profile but classified as a semimetal (see Fig. 6), is presented [32]. Notably, the EDOS intensity for

Table I
Chemical identities around each species in the amorphous configuration.

C		B		N	
C_3	51.39 %	N_2C	33.33 %	B_2C	44.44 %
BC_2	17.36 %	NC_2	30.56 %	BC_2	31.94 %
NC_2	14.24 %	N_3	15.28 %	B_3	12.50 %
BNC	7.64 %	C_3	8.33 %	C_3	6.94 %
N_2C	4.17 %	BNC	4.17 %	BC	2.78 %
B_2C	1.39 %	BN_2	2.78 %	C_2	1.39 %
BN_2	1.39 %	NC	1.39 %		
BC_3	0.69 %	BC_2	1.39 %		
B_3	0.69 %	NC_3	1.39 %		
B_2N	0.35 %	N_4	1.39 %		
BNC_2	0.35 %				
C_4	0.35 %				

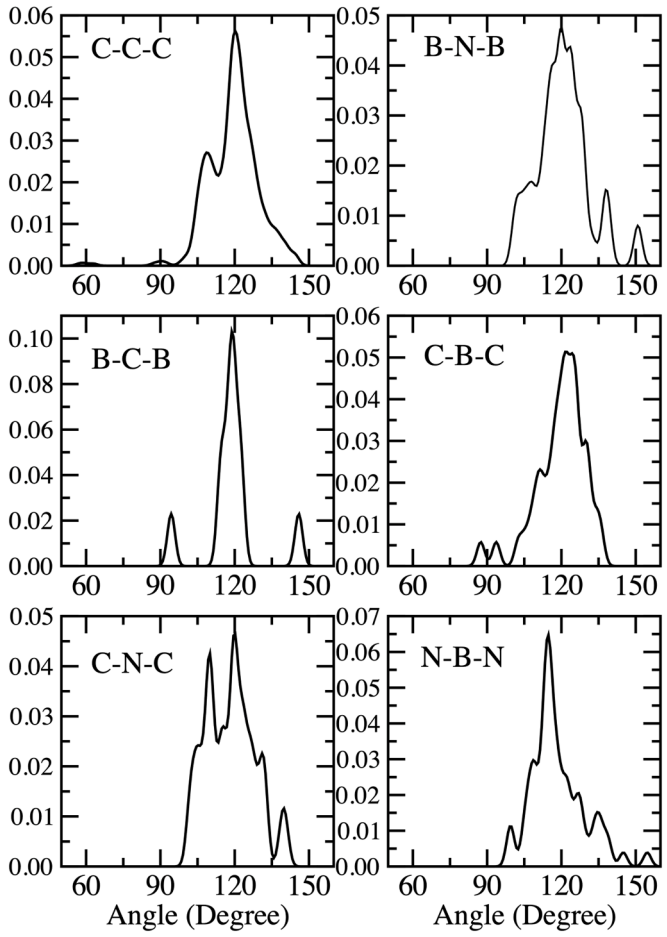

Fig. 4. Distribution of bond angles in a-BC_4N.

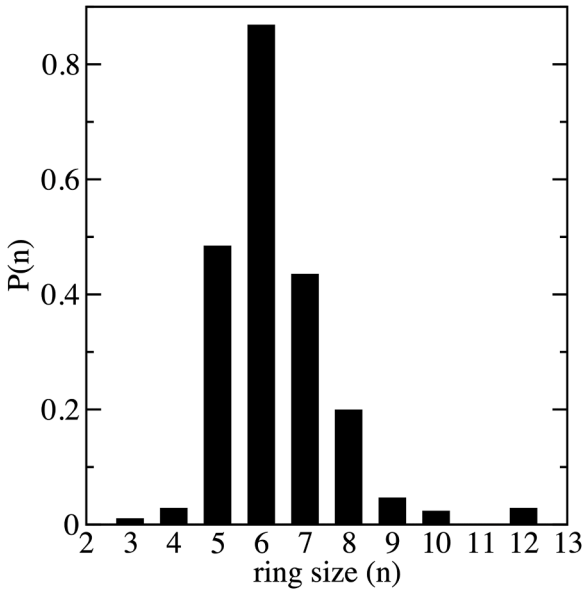

Fig. 5. Analysis of ring statistics in a-BC_4N. Here P(n) represents the fraction of nodes in a network that are part of at least one cycle of size n.

a-BC_5 near the Fermi level is higher, and its HOMO-LUMO difference is only about 0.04 eV. Based on this comparison and the observed HOMO-LUMO gap value, we can reasonably conclude that a-BC_4N exhibits characteristics of a narrow-band semiconductor.

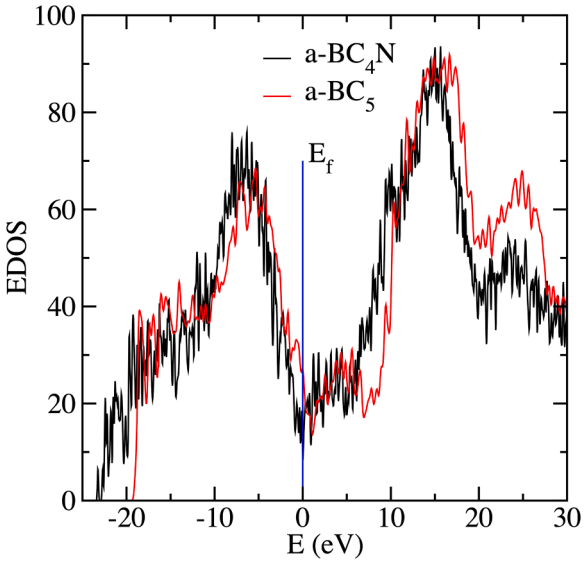

Fig. 6. Electron density of states (EDOS) of a-BC_4N and a-BC_5. The EDOS for a-BC_5 is calculated for a supercell having 432 atoms as well.

To estimate the bulk modulus (K) of a-BC_4N, we examine its energy (E) as a function of volume (V) using a variable cell optimization method, as illustrated in Fig. 7. To elucidate the energy-volume (E-V) relationship in a-BC_4N, the structure is studied under hydrostatic conditions ranging from −3 to 20 GPa, allowing both cell parameters, including shape changes, and atomic coordinates to adjust accordingly. The resulting data are subsequently fitted to the third-order Birch-Murnaghan equation of state

$$E(V) = E_0 + \frac{9V_0K}{16}\left\{\left[\left(\frac{V_0}{V}\right)^{\frac{2}{3}} - 1\right]^3 K' + \left[\left(\frac{V_0}{V}\right)^{\frac{2}{3}} - 1\right]^2 \left[6 - 4\left(\frac{V_0}{V}\right)^{\frac{2}{3}}\right]\right\}.$$

This approach yields a bulk modulus of approximately 61.81 GPa for a-BC_4N, along with a pressure derivative (K') of 7.67. For a comprehensive understanding, Table II presents a comparison between the obtained bulk modulus and other mechanical properties of a-BC_4N,

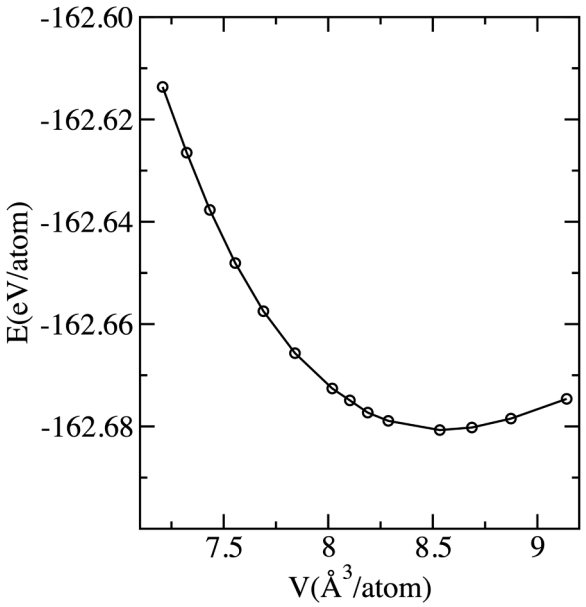

Fig. 7. Energy variation plotted against volume.

Table II
Bulk modulus (K), Young's modulus (E), shear modulus (μ), Vickers hardness (H) and Poisson ratio (ν).

Structure	K (GPa)	E (GPa)	μ (GPa)	ν	H (GPa)	References
a-BC_4N	61.81	28.8	10.12	0.42	0.027–1.53	This study
g-BC_4N	18.1 ± 0.2					[8]
g-$BC_{2.14}N$	$19.2^{\pm}0.3$					[33]
g-$BC_{1.28}N$	$20.4^{\pm}0.4$					[33]
g-BC_2N	14.63	22.81	9.20	0.24		[34]
g-BC	23					[35]
BN	36.7 ± 0.5					[36]
graphite	33.8					[37]
		25.5	9.7	0.31		[38]
	36.3	29.8	10.9	0.36	1.3	[39]
a-graphite	37.9					[40]
		28				[41]
		21				[42]
				0.28		[43]
		23–32	10–13	0.12–0.15	2–3	[44]
a-BC_5	33.9	29.2	10.8	0.35	1.63–1.85	[32]

alongside existing data for various layered structures [8,32-44]. This comparison reveals a significantly higher bulk modulus for a-BC_4N compared to all reference materials. The observed discrepancy in bulk modulus values could be attributed to the distribution of individual elements within the amorphous structure of BC_4N. This unique arrangement might contribute to a stronger resistance to compression when compared to the more ordered crystalline structure.

To calculate Young' modulus ($E = \sigma_{axial}/\varepsilon_{axial}$), controlled axial strains (ε_{axial}) are applied along the material's principal axes (*x, y* and *z*). The resulting stress (σ_{axial}) experienced by the material is recorded. The relationship between the applied stress and strain (σ_{axial} vs ε_{axial}) is depicted in Fig. 8. By analyzing the slope of these stress-strain curves, the average Young's modulus for a-BC_4N is estimated to be roughly 29 GPa. This value closely aligns with the projected range of 21–32 GPa for various layer-like materials, suggesting a similar level of stiffness between a-BC_4N and them.

The investigation extends to two further parameters that characterize a material's elastic behavior: Poisson's ratio (ν) and shear modulus (μ). They can be straightforwardly calculated from the following two equations,

$$\nu = \frac{1}{2} - \frac{E}{6K}$$

$$\mu = \frac{E}{2(1+\nu)}.$$

Theoretical predictions suggest a Poisson's ratio of around 0.42 for a-BC_4N. This value is significantly higher than the range observed in similar graphite-like structures (0.17–0.28). However, it aligns more closely with the Poisson's ratio of graphite or a-BC_5. The estimated shear modulus (μ) for a-BC_4N is nearly 10.12 GPa. This value falls within the expected range for similar materials, indicating that a-BC_4N's resistance to shearing forces is comparable to its counterparts.

To evaluate Vickers hardness of a material, several empirical relations have been proposed in the literature. Three separate equations are employed for this estimation:

$$H = 0.151\ \mu$$

$$\mathrm{H} = 0.92 \left(\frac{1}{n}\right)^{1.137} (\mu)^{0.708}$$

$$H = 0.0635\ E.$$

These equations result in a predicted Vickers hardness range for a-BC_4N between 0.027 and 1.53 GPa, falling below the value typically observed for a-graphite but aligning well with the range observed for graphite.

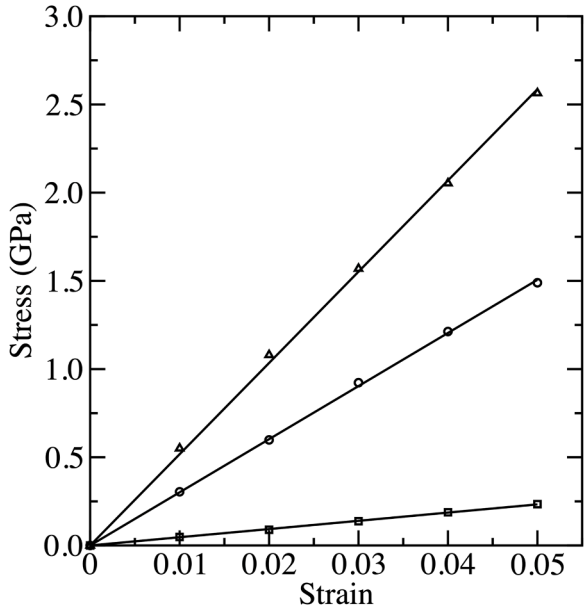

Fig. 8. The stress-strain relationship. The data points represented by circles, squares, and triangles correspond to compression along the *x, y*, and *z* axes, respectively. Notably, the observed lower stress required for compression along the y-axis aligns with the presence of stacked layers oriented in this direction, as evident in Fig. 2.

4. Conclusions

An a-BC_4N model is generated using ab initio MD simulations, and its atomic structure, mechanical, and electrical properties are investigated. Structural analysis reveals that a-BC_4N possesses a layered structure with an average layer spacing of 3.2 Å, yielding its density comparable to those reported for g-BC_4N. The configuration exhibits some coordination defects, with fourfold coordination for C and B atoms and twofold coordination for N atoms, resulting in an average coordination number of about 3.0 for all species. Further analysis suggests that a-BC_4N does not demonstrate a sandwich-like arrangement or random distribution of B, C, and N as proposed for the crystal structures, indicating a significantly distinct local structure. While C atoms dominate within each layer, there are also BN domains present. BC and CN domains appear less favorable. Despite the structural differences (distribution of atoms, coordination and structural defects etc.) from crystal structures, electronic structure calculations indicate that a-BC_4N likely behaves as a narrow-band semiconductor with band gap energy of 0.15 eV, potentially offering advantages over materials like a-graphite. In terms of mechanical

properties, a-BC_4N shows characteristics comparable to other layered structures, with the notable exception of its bulk modulus. This significantly higher resistance to compression highlights a unique aspect of a-BC_4N that warrants further exploration. Overall, this study provides valuable insights into a-BC_4N's structure and properties. While it may not necessarily surpass existing graphite-like materials in all aspects, its distinct atomic configuration, semiconducting behavior, and exceptional bulk modulus suggest potential for future research and development. It is important to acknowledge that all observations are based on a 432-atom model. While this size is considerable for ab initio simulations, potential size effects cannot be entirely discounted. To achieve a comprehensive understanding of the local structure and properties of a-BC_4N, high-fidelity simulations on larger models are crucial. In larger systems, discrepancies in the population of bonds and the prevalence of fourfold coordination motifs can be anticipated. Additionally, the formation of small BC and/or CN domains within the network might be observable.

CRediT authorship contribution statement

Murat Durandurdu: Writing – review & editing, Writing – original draft, Visualization, Validation, Methodology, Funding acquisition, Formal analysis, Conceptualization.

Declaration of competing interest

The authors declare that they have no known competing financial interests or personal relationships that could have appeared to influence the work reported in this paper.

Data availability

Data will be made available on request. The data that support the findings of this study are available on a reasonable request from the corresponding author.

Acknowledgments

The author extends gratitude to the Abdullah Gül University Support Foundation for their support. The author acknowledges the computing resources and time generously provided by TÜBİTAK ULAKBİM High Performance and Grid Computing Center (TRUBA resources).

References

[1] S.D. Nehate, A.K. Saikumar, A. Prakash, K.B. Sundaram, A review of boron carbon nitride thin films and progress in nanomaterials, Mater. Today Adv. 8 (2020) 100106–100170.
[2] R. Bahadur, G. Singh, Y. Bando, A. Vinu, Advanced porous borocarbonitride nanoarchitectonics: their structural designs and applications, Carbon. N. Y. 190 (2022) 142–169.
[3] M. Kaur, K. Singh, A. Vij, A. Kumar, Recent insights into BCN nanomaterials–synthesis, properties and applications, New. J. Chem. 47 (5) (2023) 2137–2160.
[4] M. Kawaguchi, B/C/N materials based on the graphite network, Adv. Mater. 9 (8) (1997) 615–625.
[5] Y. Li, W. Gao, F. Wang, D. Zhao, Y. Zhang, H. Yin, Self-ordered orientation of crystalline hexagonal boron nitride nanodomains embedded in boron carbonitride films for band gap engineering, Coatings 9 (2019) 185–199.
[6] M. Hubáček, T. Sato, Preparation and properties of a compound in the BCN system, J. Solid. State Chem. 114 (1995) 258–264.
[7] K. Raidongia, K.P.S.S. Hembram, U.V. Waghmare, M. Eswaramoorthy, C.N.R. Rao, Synthesis, structure, and properties of mesoporous B/C/N microspheres, Z Anorg Allg. Chem 636 (2010) 30–35.
[8] V.L. Solozhenko, V.Z. Turkevich, T. Sato, Phase Stability of Graphitelike BC4N up to 2100 K and 7 GPa, J. Am. Ceram. Soc. 80 (1997) 3229–3232.
[9] X. Luo, Z. Liu, J. He, B. Xu, D. Yu, H.T. Wang, Y. Tian, Prediction of graphitelike BC4N from first-principles calculations, J. Appl. Phys. 105 (2009) 043509–043511.
[10] Y. Zhao, D. He, L. Daemen, T. Shen, R. Schwarz, Y. Zhu, D. Bish, J. Huang, J. Zhang, G. Shen, et al., Superhard B-C-N Materials Synthesized in Nanostructured Bulks, J Mater Res 17 (2002) 3139–3145.
[11] M. Tang, D. He, W. Wang, H. Wang, C. Xu, F. Li, J. Guan, Superhard solid solutions of diamond and cubic boron nitride, Scripta Mater 66 (2012) 781–784.
[12] F. Li, Y.H. Man, C.M. Li, J.P. Wang, Z.Q. Chen, Mechanical properties, minimum thermal conductivity, and anisotropy in bc-structure superhard materials, Comput. Mater. Sci. 102 (2015) 327–337.
[13] D. Wang, R. Shi, L.H. Gan, t-C8B2N2: a potential superhard material, Chem. Phys. Lett. 669 (2017) 80–84.
[14] N.R. Qu, H.C. Wang, Q. Li, Z.P. Li, F.M. Gao, An orthorhombic phase of superhard o-BC4N, Chin. Phys. Lett. 36 (3) (2019) 036201–036205.
[15] L. Zhu, M. Ma, Q. Gao, B. Li, X. Wei, M. Xiong, Z. Zhao, J. He, Prediction of a series of superhard BC4N structures, Diamond Relat. Mater. 127 (2022) 109192–1091998.
[16] S. Bhat, P.V.W. Sasikumar, L. Molina-Luna, M.J. Graczyk-Zajac, H.J. Kleebe, R. Riedel, Electrochemical Li storage properties of carbon-rich B–C–N ceramics, C. (Basel) 2 (2016) 9–18.
[17] S. Bhat, Studies on boron-carbon-nitrides (BCN) leading to the discovery of the novel boron oxynitride B6N4O3, Ph.D. Thesis, Darmstadt, 2016.
[18] J.M. Soler, E. Artacho, J.D. Gale, A. García, J. Junquera, P. Ordejón, D. Sánchez-Portal, The SIESTA method for ab initio order-N materials simulation, J. Phys. Condens. Matter. 14 (11) (2002) 2745–2779.
[19] N. Troullier, J.L. Martins, Efficient pseudopotentials for plane-wave calculations, Phys. Rev. B 43 (1991) 1993–2006.
[20] J.P. Perdew, K. Burke, M. Ernzerhof, Generalized gradient approximation made simple, Phys. Rev. Lett. 77 (1996) 3865–3868.
[21] S. Grimme, Semiempirical GGA-type density functional constructed with a long-range dispersion correction, J. Comput. Chem. 27 (15) (2006) 1787–1799.
[22] M. Parrinello, A. Rahman, Polymorphic transitions in single crystals: a new molecular dynamics method, J. Appl. Phys. 52 (1981) 7182–7185.
[23] S. Le Roux, V. Petkov, ISAACS–interactive structure analysis of amorphous and crystalline systems, J. Appl. Crystallogr. 43 (2010) 81–85.
[24] K. Momma, F. Izumi, VESTA 3 for three-dimensional visualization of crystal, volumetric and morphology data, J. Appl. Crystallogr. 44 (2011) 1272–1276.
[25] B. Bhattarai, A. Pandey, D.A. Drabold, Evolution of amorphous carbon across densities: an inferential study, Carbon. N. Y. 131 (2018) 168–174.
[26] S.F. Parker, S. Imberti, S.K. Callear, P.W. Albers, Structural and spectroscopic studies of a commercial glassy carbon, Chem Phys 427 (2013) 44–48.
[27] Y Kumashiro (Ed.), Electric refractory materials, Taylor & Francis, New York, 2000.
[28] S. Datta, P. Singh, D. Jana, C.B. Chaudhuri, M.K. Harbola, D.D. Johnson, A. Mookerjee, Exploring the role of electronic structure on photo-catalytic behavior of carbon-nitride polymorphs, Carbon. N. Y. 168 (2020) 125–134.
[29] H. Lu, Y. Guo, J.W. Martin, M. Kraft, J. Robertson, Atomic structure and electronic structure of disordered graphitic carbon nitride, Carbon. N. Y. 147 (2019) 483–489.
[30] Q. Hu, Q. Wu, Y. Ma, L. Zhang, Z. Liu, J. He, H. Sun, H.T. Wang, Y. Tian, First-principles studies of structural and electronic properties of hexagonal BC5, Phys. Rev. B 73 (2006) 214116.
[31] D. Tomanek, R.M. Wentzcovitch, S.G. Louie, M.L. Cohen, Calculation of electronic and structural properties of BC3, Phys. Rev. B 37 (1988) 3134–3136.
[32] M. Durandurdu, Amorphous BC5 from first principles calculations, J. Non-Cryst Solids 592 (2022) 121743–121747.
[33] V.L. Solozhenko, Phase formation in the BCN system at high-pressures and temperatures: in situ studies, Eur .J. Solid State Inorg. Chem. 34 (1997) 797–807.
[34] A. Bafekry, M. Naseri, M. Faraji, M.M. Fadlallah, D.M. Hoat, H.R. Jappor, M. Ghergherehchi, D. Gogova, H. Afarideh, Theoretical prediction of two-dimensional BC2X (X= N, P, As) monolayers: ab initio investigations, Sci. Rep. 12 (1) (2022) 22269.
[35] V.L. Solozhenko, O.O. Kurakevych, E.G. Solozhenko, J. Chen, J.B. Parise, Equation of state of graphite-like BC, Solid. State Commun. 137 (5) (2006) 268–271.
[36] V.L. Solozhenko, G. Will, F. Elf, Isothermal compression of hexagonal graphite-like boron nitride up to 12 GPa, Solid. State Commun. 96 (1) (1995) 1–3.
[37] M. Hanfland, H. Beister, K. Syassen, Graphite under pressure: equation of state and first-order Raman modes, Phys. Rev. B 39 (1989) 12598–12603.
[38] J.R. Cost, K.R. Janowski, R.C. Rossi, Elastic properties of isotropic graphite, Philos Mag 17 (1968) 851–854.
[39] K. Luo, B. Liu, L. Sun, Z. Zhao, Y. Tian, Design of a class of new sp –sp carbons constructed by graphite and diamond building blocks, Chin Phys Lett 38 (2021) 028102–028107.
[40] X. Wang, Z.X. Bao, Y.L. Zhang, F.Y. Li, R.C. Yu, C.Q. Jin, High pressure effect on structural ND electrical properties of glassy carbon, J. Appl. Phys. 93 (2003) 1991–1994.
[41] M. Sakai, H. Hanyu, M. Inagaki, Indentation-induced contact deformation and damage of glasslike carbon, J. Am. Chem. Soc. 78 (1995) 1006–1012.
[42] J.S. Field, M.V. Swain, The indendation characterisation of the mechanical properties of various carbon materials: glassy carbon, coke and pyrolytic Graphite, Carbon. N. Y. 34 (1996) 1357–1366.
[43] X. Jiang, J.W. Zou, K. Reichelt, P. Grüenber, The study of mechanical properties of a-C: h films by Brillouin scattering and ultralow load indentation, J. Appl. Phys. 66 (1989) 4729–4735.
[44] H.M. Hawthorne, The micro indentation hardness behaviour of carbon filaments, glassy carbons, and pyrolytic graphites, Carbon. N. Y. 13 (1975) 215–223.